Supporting information for
Quantum-mechanical treatment of thermal effects on structure and ^{13}C NMR shielding of Buckminsterfullerene C_{60}

Tiia Jacklin,[*a] Petr Štěpánek,[a,b] and Perttu Lantto[*a]

[a] NMR Research Unit, Faculty of Science, University of Oulu, P.O. Box 3000, FI-90014 Oulu, Finland
[b] Water, Energy and Environmental Engineering Research Unit, Faculty of Technology, University of Oulu, P. O. Box 4300, FI-90014, Finland
[*] Corresponding author, e-mail: tiia.jacklin@oulu.fi, perttu.lantto@oulu.fi

Contents

1 Structural and volume changes of C_{60}

1.1 Volume and the volumetric thermal expansion coefficient

The volume of C_{60} at different temperatures was extracted from the corresponding effective geometries computed with the Dalton code [1, 2]. The fullerene was treated as an ellipsoid, and the volume is computed from the eigenvalues of the gyration tensor (λ_i)[3]:

$$V = 4\sqrt{3}\pi \prod_{i=1}^{3} \sqrt{\lambda_i}. \tag{1}$$

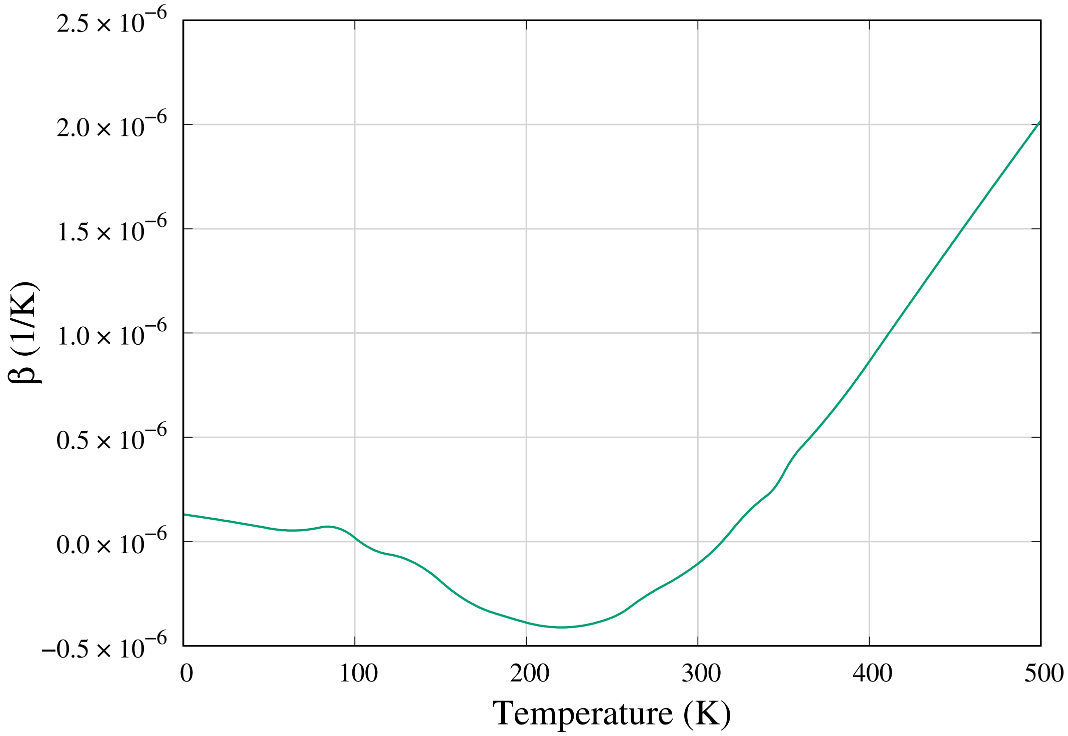

Figure S1: Temperature dependence of the volumetric thermal expansion coefficient, $\beta(T)$. The values are available in the Excel file on sheet 'Thermal_expansion_coefficient'.

Volume data enables computing temperature dependence of the volumetric thermal expansion coefficient as

$$\beta(T) = \frac{1}{V}\frac{dV}{dT}, \tag{2}$$

which is plotted in Fig. S1. To get better estimates for the temperature derivative in Eq. (2), volume data was interpolated with CubicSpline function of scipy.interpolate module in Python. As seen in Fig. S1, the β is positive at low temperatures below $T = 100$ K, where volume increases monotonically due to linearly temperature-dependent centrifugal distortion effects (CTE) (see Eq. (1) of the article). The anharmonic vibrational contributions to effective geometry of all normal modes remain $T = 0$ K values until $T = 100$ K, where their decreasing volume effect overcomes the increasing CTE effect and β coefficient becomes negative. The minimum value of $\beta = -0.411 \times 10^{-6}$ 1/K is reached around $T = 220$ K. The β becomes positive again at $T = 320$ K, where the volume of fullerene is at a minimum, and it then increases linearly up to the highest computed temperature $T = 500$ K. The temperature dependence of β coefficient is quite different from the one obtained with classical MD simulations by Kwon *et. al.* [4], where the positive region at low temperatures is absent, NTE starts from at $T = 0$ K and the minimum is reached already below $T = 100$ K. Also, we do not observe the strongly nonlinear behavior at high temperatures, and the expansion is an order of magnitude smaller than in the classical MD study[4].

1.2 Normal mode analysis of the effective geometry corrections

Normal mode analysis is carried out for fully ^{12}C C$_{60}$ isotopomer with icosahedral I_h symmetry. The effective geometry corrections in normal modes and their relative changes with respect to the values of $T = 0$ K are displayed in Fig. S2 and Fig. S3, respectively. The vibrational and CTE contributions of mode number 148, which is the non-degenerate, Raman active, fully symmetric, radial A$_\mathrm{g}$(1) mode, are among the contributions listed for all vibrational normal modes and isotopomers in the Excel file on sheets 'Effective_geometry_vibrational', 'Effective_geometry_centrifugal' and 'Effective_geometry_total'.

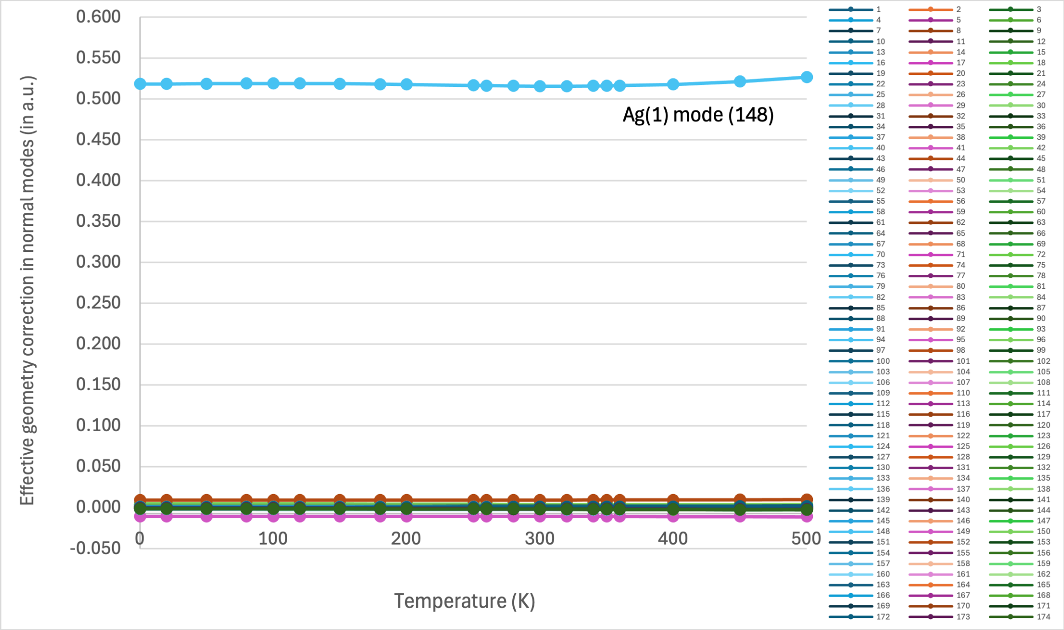

Figure S2: The effective geometry corrections in normal modes.

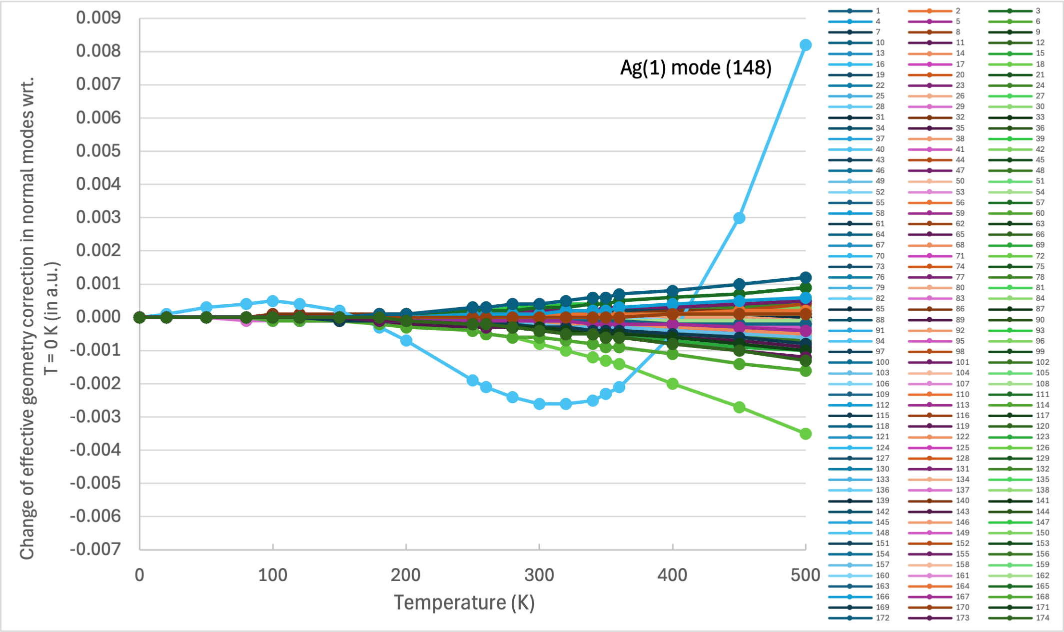

Figure S3: The relative changes of effective geometry corrections in normal modes with respect to the values at $T = 0$ K.

1.3 Temperature dependence of bond lengths

The temperature dependence of the HH and HP bond lengths are shown in Fig. S4 as averages over all HH and HP bonds. The temperature dependence of HP bonds is similar to the whole structure, whereas HH bonds shorten also at higher temperatures, where NTE is no longer happening.

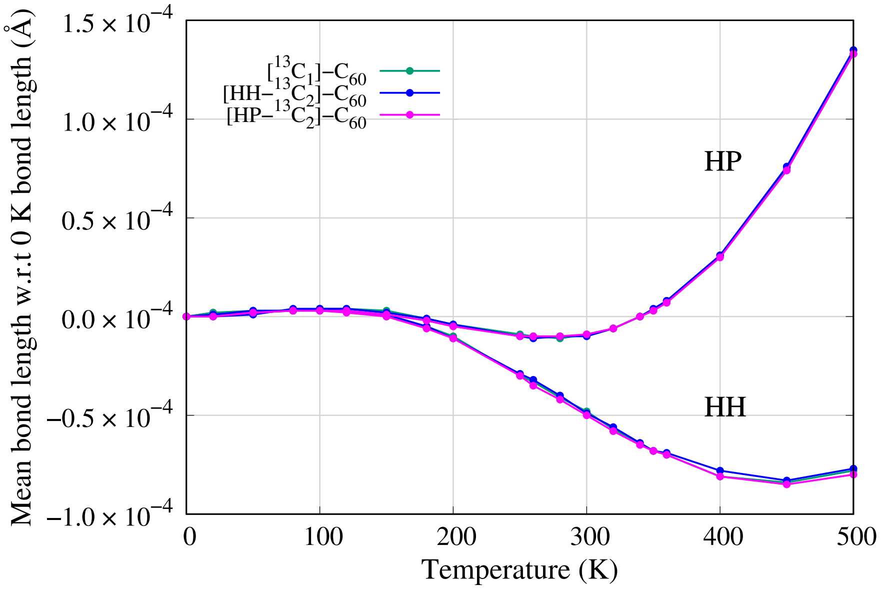

Figure S4: Temperature dependence in different isotopomers of bond lengths with respect to their $T = 0$ K values for average bond lengths computed over the whole C_{60} structure.

2 ^{13}C NMR shielding and isotope shifts

2.1 ^{13}C NMR shielding in fullerene C$_{60}$

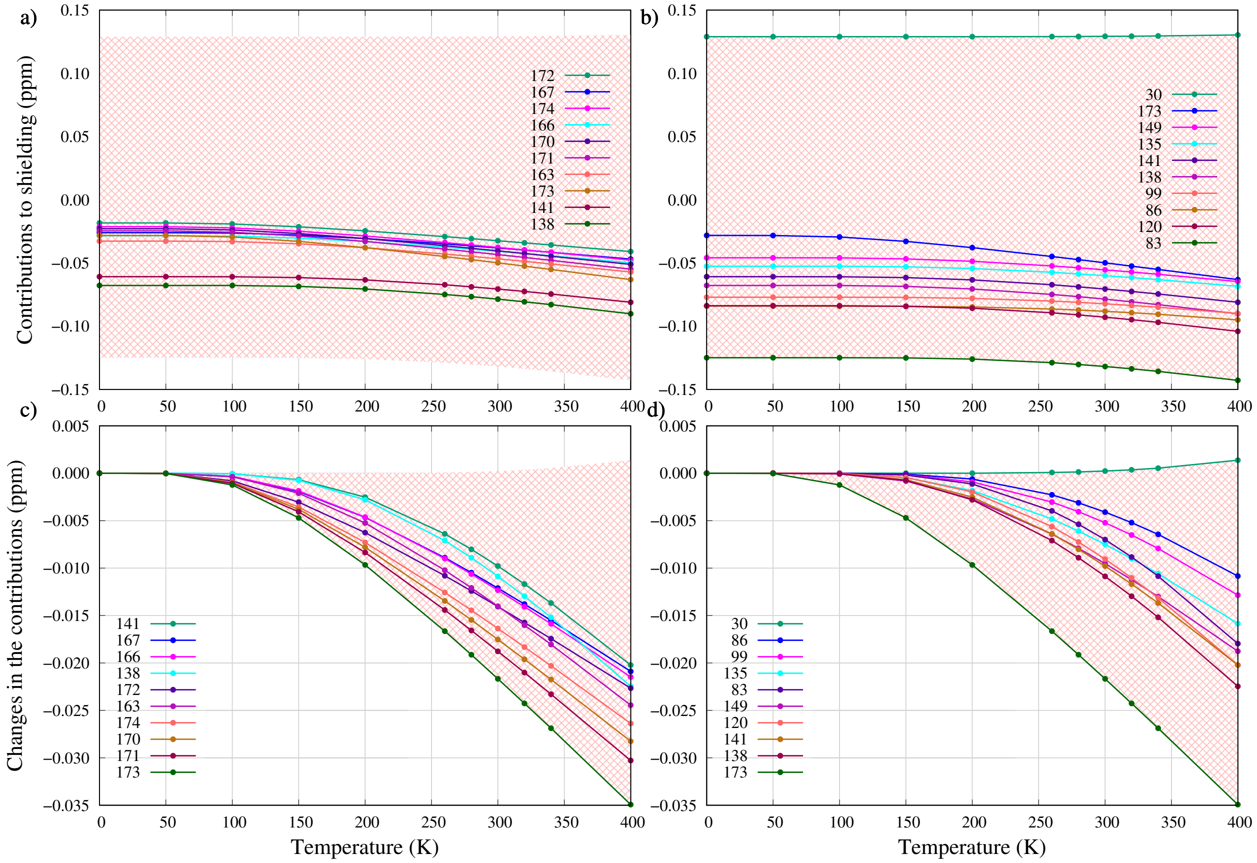

Figure S5: Temperature dependence of the harmonic vibrational corrections in normal modes to the ^{13}C shielding in $[^{13}\mathrm{C}_1] - \mathrm{C}_{60}$ isotopomer. a) 10 most T-dependent modes. b) 10 modes with largest absolute values. c) and d) panels, respectively, show the corresponding temperature dependence with respect to the $T = 0$ K value. The colored area indicates the region of all normal mode contributions. Numbering of modes is according to Dalton code, and the values are available in the Excel file on the sheet '13C_shielding_contributions'.

2.2 ^{13}C shielding in reference methane CH_4 molecule

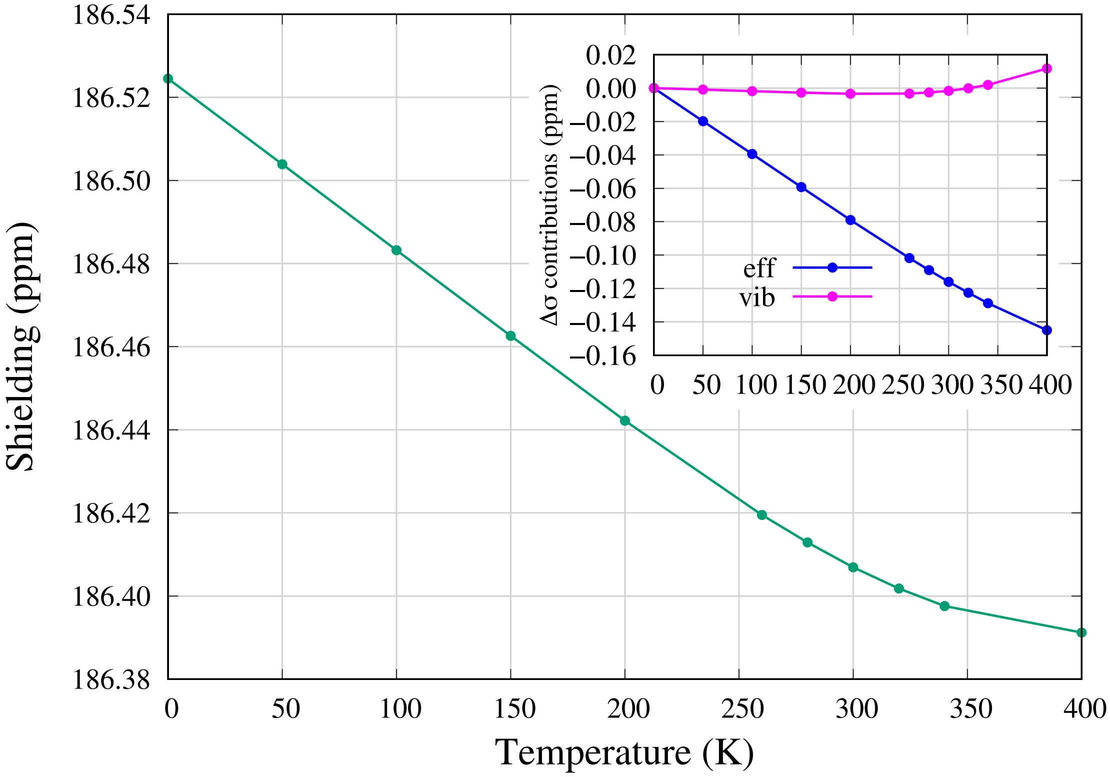

Figure S6: Shielding of ^{13}C in CH_4. The effective geometry contributions (eff) and vibrational contributions (vib) are given with respect to their 0 K values in the inset. The absolute values can be found in the Excel file on sheet 'Shielding_of_C60_and_CH4'.

The computed shielding of ^{13}C in methane CH_4 can be found in Fig. S6. Methane shielding decreases linearly about -0.1 ppm at $T = 0 \ldots 300$ K range due to lengthening of the C-H bonds. This is caused by centrifugal distortion effect (CDE) on effective geometry (eff). Around room temperature both anharmonic vibrational effect on effective geometry (eff) and harmonic vibrational correction to shielding (vib) become important and cause nonlinear change of shielding, which slows down temperature dependence at high temperatures.

2.3 ^{13}C chemical shift of C_{60} with respect to the reference methane CH_4 molecule

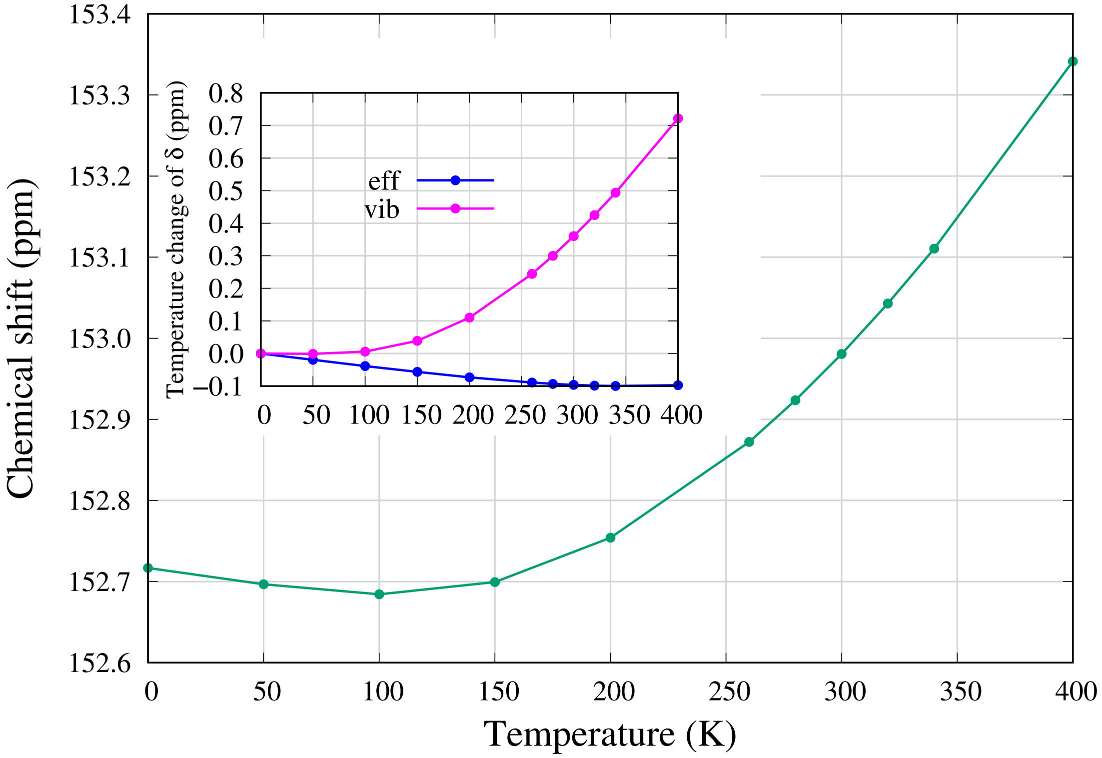

Figure S7: Temperature dependence of the ^{13}C chemical shift, $\delta_{\mathrm{C}_{60}}$, of the main $[^{13}\mathrm{C}_1]-\mathrm{C}_{60}$ isotopomer with respect to methane, $^{13}CH_4$. The effective geometry (eff) and vibrational (vib) contributions are given with respect to their $T = 0$ K values in the inset.

Temperature dependence of the ^{13}C NMR chemical shift in the $[^{13}\mathrm{C}_1]-\mathrm{C}_{60}$ isotopomer with respect to methane, $^{13}CH_4$, reference molecule, $\delta_{\mathrm{C}_{60}} = \sigma_{\mathrm{CH}_4} - \sigma_{\mathrm{C}_{60}}$, is shown in Fig. S7. The main peak moves between $152.7 - 153.3$ ppm at temperatures between 0-400 K. The small decrease in $\delta_{\mathrm{C}_{60}}$ in low temperatures is due to the monotonic decrease of $^{13}CH_4$ shielding due to effective geometry contribution (see Fig. S6), until harmonic vibrational contributions to C_{60} above $T = 100$ K outgrow it.

The temperature derivative of ^{13}C chemical shift, $(d\delta_{\mathrm{C}_{60}}/dT) = 2.71 \times 10^{-3}$ ppm/K, in $240 - 300$ K temperature interval is slightly larger than experimentally observed one, 1.88×10^{-3} ppm/K [5]. A major difference is that the experimental observation is carried out for a solid-state sample with intermolecular interactions, while our value is modeled for a single molecule without external interactions corresponding to a low-density gas phase. The magnitude of the temperature derivative of pure isotropic shielding without the decreasing effect of reference CH_4 shielding (see Fig. S6), is even slightly larger, $(d\sigma_{\mathrm{C}_{60}}/dT) = -3.02 \times 10^{-3.02}$ ppm/K.

2.4 Secondary isotope shifts

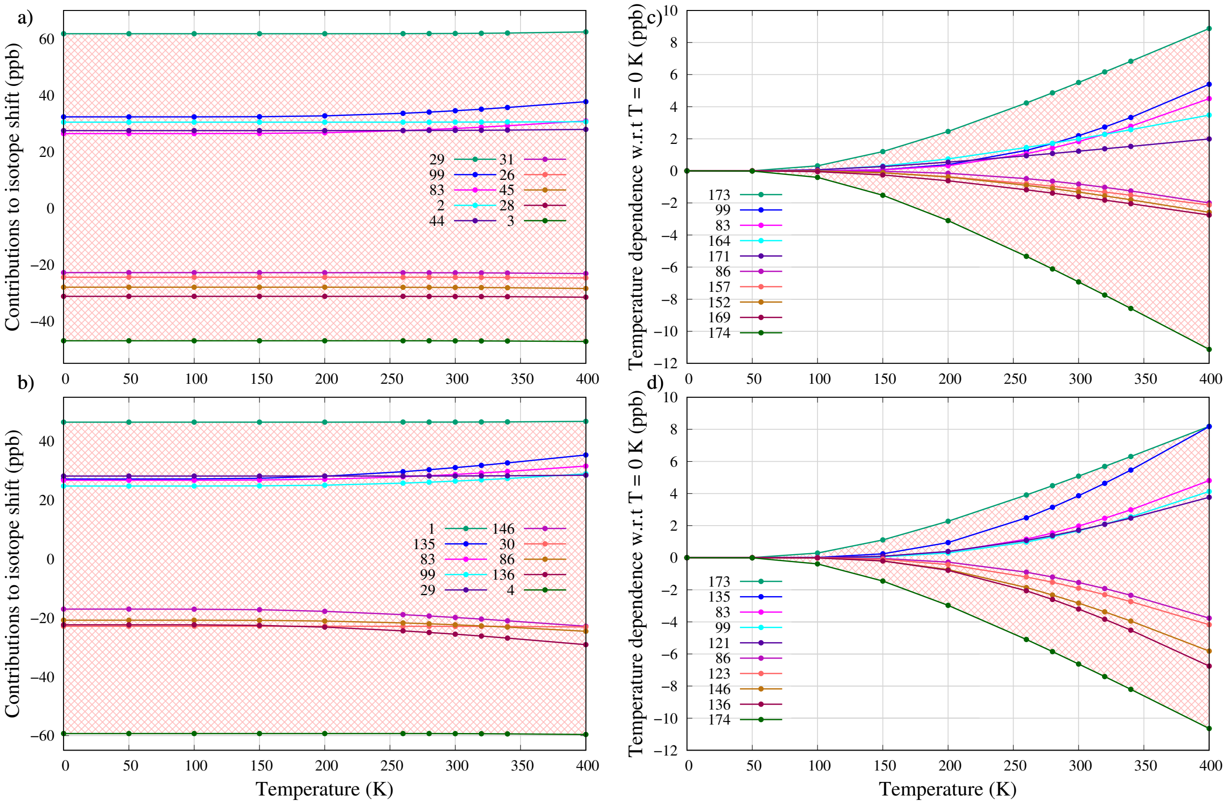

Figure S8: The absolute (left) and relative to $T = 0$ K (right) contributions (in ppb) to a,c) ${}^{1}\Delta_{\mathrm{HP}}$ and b,d) ${}^{1}\Delta_{\mathrm{HH}}$ isotope shifts from vibrational normal modes. The colored area indicates the region in which the contributions of all modes are. Ten normal modes with the largest absolute and relative contributions are shown with numbering according to Dalton code. The values of the isotope shifts are available in the Excel file on sheet 'Isotope_shifts' and the contributions from vibrational normal modes on the sheets 'HH_shielding_contributions' and 'HP_shielding_contributions'.

The following isotope shifts are calculated and compared with the experimental results by Bacanu *et al.*[6]

$$
\begin{aligned}
{}^{1}\Delta_{\mathrm{HH}} &= \delta^{{}^{13}\mathrm{C}}\left([{}^{13}\mathrm{C}_1]-\mathrm{C}_{60}\right) - \delta^{{}^{13}\mathrm{C}}\left([\mathrm{HH}-{}^{13}\mathrm{C}_2]-\mathrm{C}_{60}\right) &\quad (3)\\
{}^{1}\Delta_{\mathrm{HP}} &= \delta^{{}^{13}\mathrm{C}}\left([{}^{13}\mathrm{C}_1]-\mathrm{C}_{60}\right) - \delta^{{}^{13}\mathrm{C}}\left([\mathrm{HP}-{}^{13}\mathrm{C}_2]-\mathrm{C}_{60}\right) &\quad (4)
\end{aligned}
$$

2.5 Functional and basis set tests

The main results of the article were obtained with hybrid PBE0 functional [7, 8] and the best affordable pcSseg-1 basis set [9]. In order to find out the sensitivity of the thermal effects on structure and NMR parameters to the quality of DFT functional, also PBE[7] functional, not including the 25% of Hartree-Fock exact exchange, was used. Additionally, we studied the effect of smaller pcseg-1 [10] and pcSseg-0 [9] basis sets. The pcSseg-2 basis set [9] was too large for rovibrational averaging and, hence, we tested if extra d-type polarization function in pcSseg-1 basis set would affect the results. Unfortunately, it caused worse SCF convergence due to linear dependencies leading to too large numerical errors in thermal averaging and was therefore not used.

The effects of different DFT functional and basis set combinations on relative volumes are shown in Fig. S9 for isotopomer with one ^{13}C atom as others behave similarly. At low temperatures, no differences are observed since the vibrational modes are inactive, and therefore differences do not appear until at $T = 200$ K. Clearly, the very modest pcSseg-0 basis set overestimates the NTE, and the effect is greater with the hybrid PBE0 functional. Unsurprisingly, the pcseg-1 basis set gives quite similar PBE results as the pcSseg-1 basis set with better p-orbital description. Undoubtedly, the exact exchange contribution in the PBE0 functional is important for effective geometry as the NTE minimum is deeper, and it shifts towards higher temperatures. The positive thermal expansion is not so rapid at high temperatures as with the pure PBE functional.

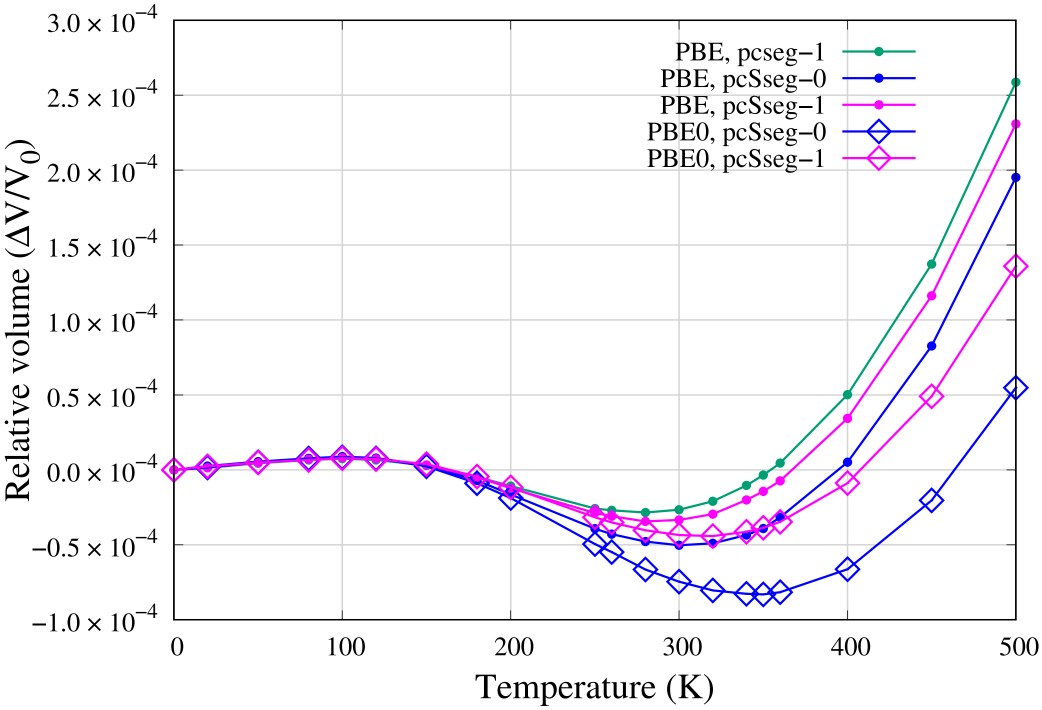

Figure S9: The relative volume $\Delta V/V_0 = (V - V_0)/V_0$ for C_{60} with one ^{13}C with different functional/basis set combinations. The values used are available in the Excel file on sheet 'Relative_volumes'.

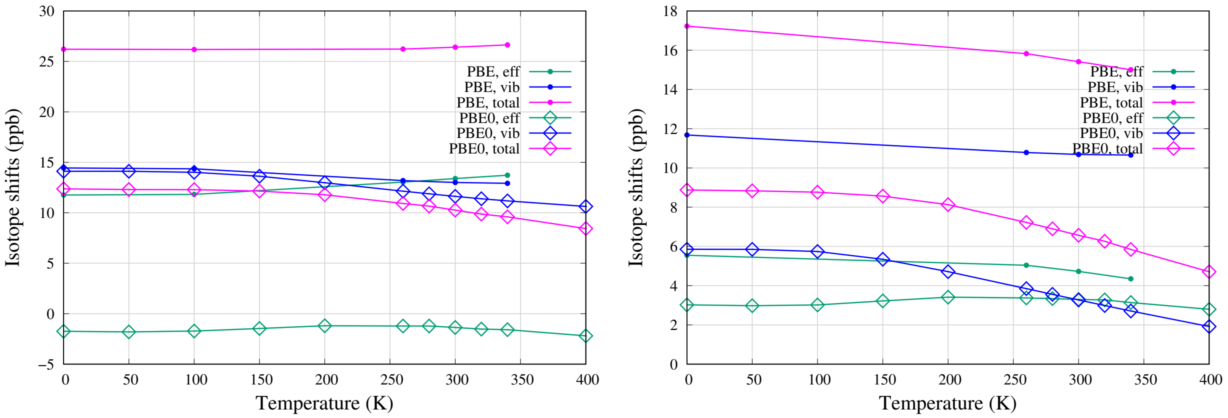

Figure S10: Difference between PBE and PBE0 functionals in the HH (left) and HP (right) isotope shifts with pcSseg-1 basis set. The effective geometry contributions (eff), vibrational contributions (vib), and total isotope shift (total) are included. The values are available in the Excel file on sheet 'Isotope_shifts'.

As seen in Fig. S10, the difference between the PBE and PBE0 functionals is much larger for isotope shifts than for the volume of C_{60} in Fig. S9. The PBE functional produces much larger isotope shifts. In the HH isotope shift, the effective geometry contribution (eff) is overestimated, and in the HP isotope shift, also the harmonic vibrational contribution (vib). In particular, the PBE functional gives incorrect temperature dependence, which is most obvious in the HH isotope shift around room temperature that increases due to a large and positive effective geometry contribution (eff). The positive derivative of the effective geometry (eff) contribution to HH isotope shift at PBE/pcSseg-1 level is due to the opposite temperature dependence of the main $A_g(1)$ mode (number 148) in HH isotopomer with respect to the other two isotopomers. This is not observed at the best PBE0 / pcSseg-1 level, which is qualitatively in agreement with the experimental results.

The isotope shifts computed with different basis sets using the PBE functional are shown in Fig. S11. Obviously, the added flexibility in p basis functions of pcSseg-n compared to pcseg-n basis sets is needed for qualitatively correct T-dependence of HP isotope shift. However, the HH isotope shift reveals that the lowest level pcSseg-0 basis set cannot describe these sensitive properties, and pcSseg-1 is a bare minimum.

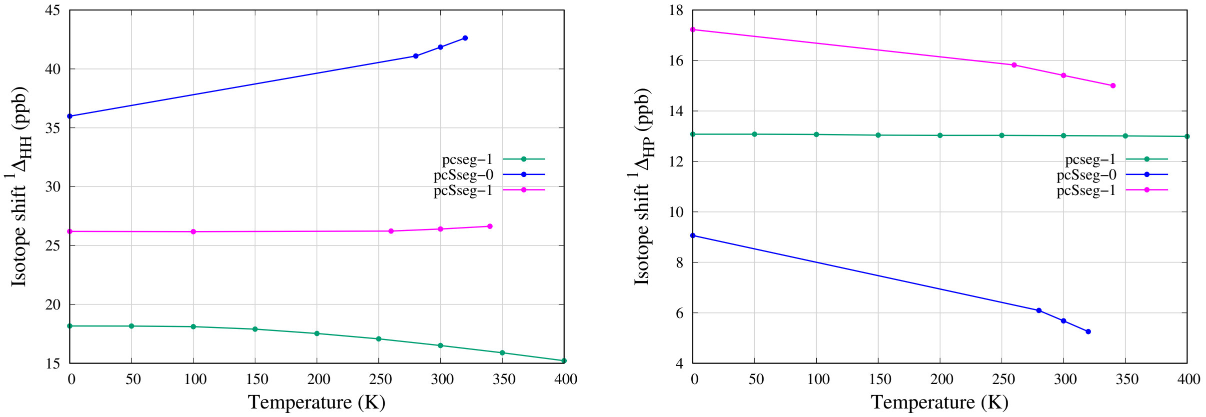

Figure S11: Difference between the basis sets in the total isotope shifts for HH-isotopomer (left) and HP-isotopomer (right) with PBE functional.

References

[1] K. Aidas, C. Angeli, K. L. Bak, V. Bakken, R. Bast, L. Boman, O. Christiansen, R. Cimiraglia, S. Coriani, P. Dahle, et al., *WIREs Comput. Mol. Sci* **2014**, *4*, 269–284.

[2] Dalton, a molecular electronic structure program, Release v2020.1 (2022), see `http://daltonprogram.org`.

[3] S. Hadizadeh, A. Linhananta, S. S. Plotkin, *Macromolecules* **2011**, *44*, 6182–6197.

[4] Y.-K. Kwon, S. Berber, D. Tománek, *Physical Review Letters* **2004**, *92*, 015901.

[5] H. He, J. T. Dias, J. Foulkes, J. Klinowski, *Physical Chemistry Chemical Physics* **2000**, *2*, 2651–2654.

[6] G. R. Bacanu, G. Hoffman, M. Amponsah, M. Concistrè, R. J. Whitby, M. H. Levitt, *Physical Chemistry Chemical Physics* **2020**, *22*, 11850–11860.

[7] J. P. Perdew, M. Ernzerhof, K. Burke, *The Journal of Chemical Physics* **1996**, *105*, 9982–9985.

[8] C. Adamo, V. Barone, *The Journal of Chemical Physics* **1999**, *110*, 6158–6170.

[9] F. Jensen, *J. Chem. Theory Comput.* **2015**, *11*, 132–138.

[10] F. Jensen, *J. Chem. Theory Comput.* **2014**, *10*, 1074–1085.